Journal of Computational Biophysics and Chemistry

Research

Cite This: *J. Comput. Biophys. Chem.* **2024**, *23* (10), 1325–1338

Cobalt(II) Complex Constructed from Pyrazinecarboxamide and Aromatic Carboxylic Acid: Synthesis, Single Crystal XRD Along with Computational Study

Melike Nur Deniz[*], Muhammad Ashfaq[†,††], Seyhan Ozturk[‡], Egor Novikov[§], Muhammad Nawaz Tahir[†], Saltanat Arshad Aghayeva[¶], Mohammad Shahidul Islam[‖], Necmi Dege[*], Tahani Mazyad Almutairi[‖] and Suraj N. Mali[**]

[*]*Department of Physics, Faculty of Science, Ondokuz Mayıs University, Atakum, 55200, Samsun, Turkey*
[†]*Department of Physics, University of Sargodha, Sargodha, 40100, Punjab, Pakistan*
[‡]*Department of Chemistry, Faculty of Science, Ondokuz Mayıs University, Atakum, 55200, Samsun, Turkey*
[§]*Department of Chemistry, New Mexico Highlands University, Las Vegas, New, Mexico, 87701, USA*
[¶]*Department of Life Sciences, Western Caspian University, Baku, Azerbaijan*
[‖]*Department of Chemistry, College of Science, King Saud University, P.O. Box 2455, Riyadh 11451, Saudi Arabia*
[**]*School of Pharmacy, DY Patil Deemed to be University Sector 7, Nerul, Navi Mumbai, 400706, India*

[††]Corresponding author. E-mails: *ashfaq.muhammad@uos.edu.pk; muhammadashfaq1400@gmail.com*

ABSTRACT: A cobalt (II) mononuclear complex was synthesized by two-nitrobenzoic acid and pyrazine-two-carboxamide ligands in the presence of sodium bicarbonate and aqueous solution of cobalt acetate tetrahydrate. The synthesized cobalt(II) complex was characterized by single crystal X-rays diffraction. The coordination geometry of the cobalt complex was octahedral with water molecules occupying the axial sites. A lot of intermolecular interactions were in response to stabilize the supramolecular assembly which were inspected by Hirshfeld surface analysis. Enrichment ratios were calculated to find the pair of atoms having the highest propensity to form crystal packing interactions. Void analysis was conducted to forecast how the crystal would respond to applied stress. Interaction energy calculations were carried out using the B3LYP/6-31G(d,p) electron density model to identify which energy types most significantly contributed to the supramolecular assembly. Moreover, the energy data obtained from DFT calculations showed an average level of stability of the molecule. The moderate HOMO-LUMO energy gap suggested reactivity, while a high electrophilicity index indicates a strong tendency for electron-accepting reactions.

KEYWORDS: Pyrazine derivative; mononuclear cobalt(II) complex; single crystal X-ray diffraction analysis; hirshfeld surface analysis; DFT.

1. INTRODUCTION

For decades, researchers have been synthesizing new coordination compounds from the ligands as the biological activities of the coordination complexes are better than the biological activities of the free ligands.[1–3] Pyrazinecarboxamide is widely used as a ligand in the synthesis of coordination complexes because of its two nitrogens and oxygen which can act as donor sites for the metals. Various coordination modes of the pyrazinecarboxamide are reported in literature, mono-dentate,[4–7] bidentate by oxygen and one of its nitrogen,[8–10] bridging[11,12] as shown in Fig. 1. According to Cambridge structural database CSD 2024.1 (updated March 2024),[13] 74 crystal structures of the metal complexes (mono nuclear, multinuclear, polymeric) are reported in literature till date that contained pyrazinecarboxamide ligand along with one or more co-ligands. 12 out of 74 structures contained cobalt metal. Three polymeric[14–16] and

Received: 3 August 2024
Accepted: 15 August 2024
Published: 28 September 2024

DOI: 10.1142/S2737416524500455
J. Comput. Biophys. Chem. **2024**, *23* (10), 1325–1338

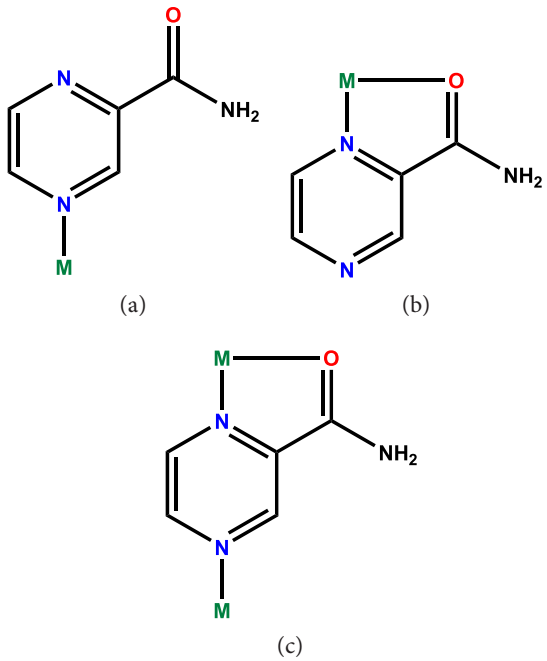

Fig. 1. (Color online) Coordination modes of pyrazinecarboxamide ligand with metals through (a) nitrogen, (b) nitrogen and oxygen, and (c) both nitrogens and oxygen.

nine nonpolymeric structures[17–19] containing pyrazinecarboxamide ligand and a co-ligand coordinated with cobalt metal are reported. Pyrazinecarboxamide-containing compounds find diverse applications across various fields, including their use as corrosion inhibitors,[20] violet and ultraviolet luminescence production upon excitation by ultraviolet light,[14] antimycobacterial,[21] antiviral,[22] electrocatalytic agents,[23] dyes[24] and drugs. The luminescence properties of a ligand can either increase or decrease upon coordination with a metal center, and this outcome depends on the different factors pertaining to the ligand's nature, the metal and their interaction.[25–27] Deprotonated aromatic carboxylic acid especially two-nitrobenzoic acid can act as monodentate, bidentate and chelating ligand for various metals.[28–32] As a result of the coordination of two-nitrobenzoate ligand with various derivatives of pyrazinecarboxamide ligands, the number of coordination geometries are reported from four-coordinated to eight-coordinated.[4,7,29,33–38] Based on our specialty on single crystal XRD and computational study of the metal complexes,[39–42] we are going to report the synthesis, single crystal XRD characterization, examination of the supramolecular assembly through Hirshfeld surface analysis and detailed computational study of the cobalt complex constructed from pyrazine derivative (pyrazinecarboxamide) and aromatic carboxylic acid (two-nitrobenzoic acid).

2. EXPERIMENTAL

2.1. Materials and methods

Starting materials and all chemical reagents for synthesis were obtained from Merck and used without further purification.

2.2. Synthesis of $[Co(NB)_2(Pyz)_2(H_2O)_2]$

In 20 ml hot distilled water, two-nitrobenzoaic acid (0.33 mg, 2 mmol) was added and stirred. The sodium bicarbonate (0.17 mg, 2 mmol) was added step by step and stirring continued for 15 min. The resulting solution was filtered and aqueous solution of cobalt acetate tetrahydrate (0.25 mg, 1 mmol) was added to the former solution. The solution of pyrazine-two-carboxamide (0.25 mg, 2 mmol) in water was added step by step to the previously obtained solution. The resulting solution was stirred at rt. for 18 h, hot water was added and sodium acetate was filtered off. It was left for four to five days to obtain blue prism-like crystals (Scheme 1) (yield = 0.44 g, 65%).

2.3. Single crystal X-ray diffraction analysis procedure

The appropriate quality crystal selected by optical microscope was inserted into STOE *IPDS* 2 diffractometer for data collection. For the structure solution, SHELXT 2014[43] was used and SHELXL 2019/2[44] was used for refinement. Disorder was observed and resolved in the nitro group of X-ray crystal structure by the usage of appropriate restraints. Hydrogen atoms were placed by using the ridding model except for hydrogens of the amino group which were freely refined for correct orientation. PLATON[45] and Mercury 4.0[46] software represented results in the form of figures.

2.4. Computational details

The study employed Density Functional Theory (DFT) via the B3LYP method with the 6-31G(d,p) basis set, utilizing Gaussian 16W[47] and GaussView 6.1 software.[48] Initially, the experimental geometry, sourced in CIF format, was converted to MOL2 format using Mercury 2024.1.0 (build 401958).[46] This format transition facilitated the importation of the geometry into GaussView 6.1.[48] Following importation, Gaussian's optimization algorithm refined the geometry for enhanced accuracy. Subsequently, Gaussian's energy calculation algorithm was engaged to derive energy

DOI: 10.1142/S2737416524500455
J. Comput. Biophys. Chem. **2024**, *23*(10), 1325–1338

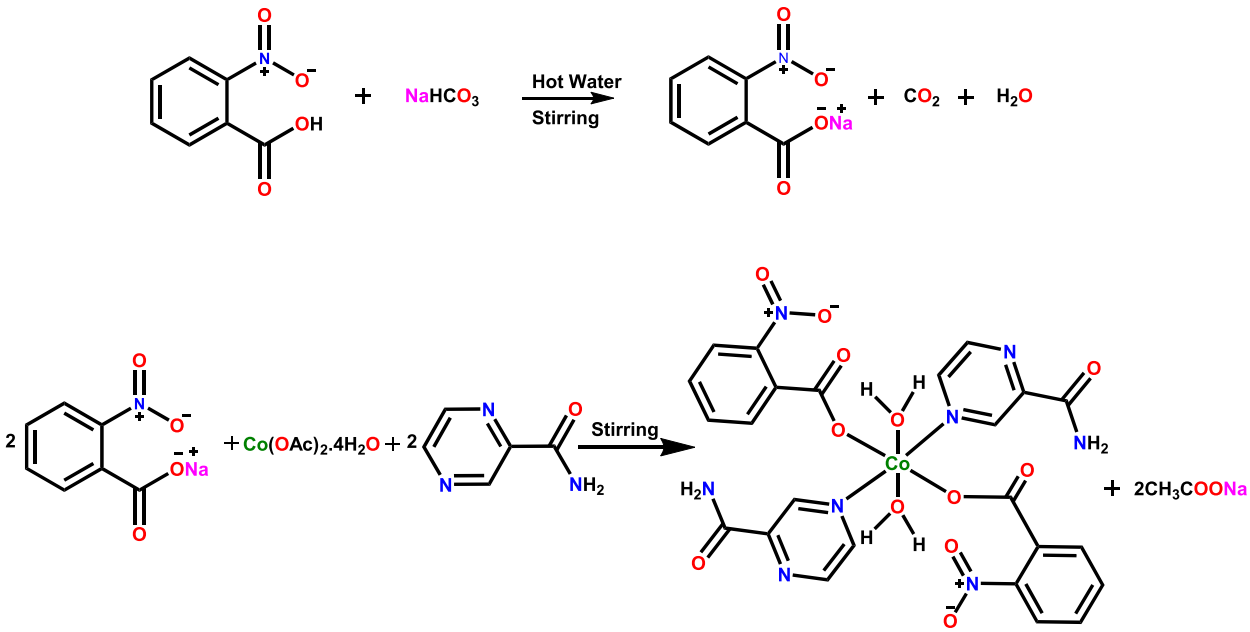

Scheme 1. (Color online) Synthesis pathway for the preparation of $[Co(NB)_2(Pyz)_2(H_2O)_2]$ complex.

values for both the frontier molecular orbitals and the entire molecular structure. Additionally, the software computed the dipole moment, which is crucial for understanding molecular polarity. Visualizing frontier molecular orbitals aided in comprehending their spatial distribution and characteristics. To further analyze the molecule's properties, molecular electrostatic potential mapping was conducted using GaussView 6.1's contour builder tool.[48] This process facilitated the visualization and interpretation of electrostatic potential surfaces, providing insights into molecular reactivity and intermolecular interactions.

3. RESULTS AND DISCUSSIONS

3.1. Single crystal XRD exploration

The lattice parameters along with other important details are listed in Table 1. The asymmetric unit of the cobalt complex $[Co(NB)_2(Pyz)_2(H_2O)_2]$ (Fig. 2) has half a molecule and the completion of the molecule is due to the inversion symmetry. Cobalt center is coordinated by two-nitrobenzoate by one of its O-atom of benzoate, pyrazinecarboxamide by one of its nitrogen and water ligands. The coordination fashion of the two-nitrobenzoate and pyrazinecarboxamide ligands is similar to nonchelating. Cobalt center is hexacoordinated and octahedral geometry is formed in which water O-atoms occupy axial sites while the remaining atoms of the coordination sphere occupy equatorial sites. The equatorial coordination plane makes the dihedral angles of 38.1 (1) and 84.7 (2)° with root mean square plane of the pyrazine ring and carboxylate group, respectively. The twist between pyrazine and phenyl ring is 87.2 (8)°. Pyrazinecarboxamide is planar with root mean square deviation of 0.0223 Å whereas two-nitrobenzoate ligand is nonplanar. The carboxylate group, major and minor parts of the nitro group are orientated at dihedral angles of 20.9 (3)°, 60.2 (3)° and 52.9 (3)° with respect to the phenyl ring. The configuration of the molecule is stabilized by O–H···O and N–H···N bonding (Table 2). The molecules are connected in the form of dimers through O–H···O and N–H···N bonding (Fig. S1, Table 2). Amino group, carbonyl O-atom of pyrazinecarboxamide and non-coordinating O-atom of benzoate are involved in H-bonding. Water molecule and amino group played important roles in the crystal packing as both hydrogen of the amino group and water participate in H-bonding. A significant role in supramolecular assembly is also played by C–H···π interaction (Fig. 3, Table 2). Very weak $\pi\cdots\pi$ interactions are found with inter-centroid separation of 4.33 to 4.49 Å.

The literature survey was performed by using the Cambridge structural database CSD 2014.1 (updated March 2024).[13] Two copper complex structures containing two-nitrobenzoic acid and pyrazine-two-carboxamide ligands are found with reference codes DIFKAG[4] and DIFKAG01.[7] The coordination mode of the ligands with copper metal in these reported

DOI: 10.1142/S2737416524500455
J. Comput. Biophys. Chem. **2024**, *23* (10), 1325–1338

Table 1. Important experimental particulars of $[Co(NB)_2(Pyz)_2(H_2O)_2]$.

CCDC	2102866
Chemical formula	$C_{24}H_{22}CoN_8O_{12}$
M_r	673.42
Crystal system, space group	Monoclinic, $P2_1/n$
Temperature (K)	293
a, b, c (Å)	7.7371 (3), 19.2601 (9), 9.9276 (4)
β (°)	107.955 (3)
V (Å^3)	1407.34 (11)
Z	2
Radiation type	Mo $K\alpha$
Wavelength (Å)	0.71073
Color and shape of crystal	Light brown rod
μ (mm^{-1})	0.69
Crystal size (mm)	0.44×0.22×0.20
Diffractometer	STOE *IPDS* 2
Absorption correction	Integration STOE *X-RED*
No. of measured, independent and observed [$I>2\sigma(I)$] reflections	20980, 2936, 2464
R_{int}	0.052
$(\sin\theta/\lambda)_{max}$ (Å^{-1})	0.630
$R[F^2>2\sigma(F^2)]$, $wR(F^2)$, S	0.043, 0.116, 1.06
No. of reflections	2936
No. of parameters	206
H-atom treatment	H atoms treated by a mixture of independent and constrained refinement
$\Delta\rho_{max}$, $\Delta\rho_{min}$ (e Å^{-3})	0.56, −0.43

structures is similar to the coordination mode of the ligands with cobalt metal in our structure. The structure with reference code DIFKAG01 is the polymorph of the structure with reference code DIFKAG. The dihedral angle between pyrazine and phenyl ring is 81.79 (1) and 81.90 (2)° in DIFKAG and DIFKAG01, respectively. No other metal structure is reported containing two-nitrobenzoic acid and pyrazine-two-carboxamide ligands. In order to find more related structures, a search was performed for structures containing two-nitrobezoate, pyrazine and any metal. A crystal structure of the copper complex is reported in the literature that contained nitro group at third and fifth positions of benzoate group with reference code DIFJUZ.[4] The dihedral angle between pyrazine and phenyl ring is 58.01 (1)° in DIFJUZ. Four silver polymeric structure complexes containing substituted pyrazine ligand were reported in the literature with reference codes AJIPAM,[29] HATSUT,[33] KEXPIP[34] and TAYZIF.[37] Moreover, related dinuclear cadmium complex and polymeric manganese structures were reported with reference codes XICTOV[38] and NULLEN,[35] respectively. The bond lengths and bond angles of $[Co(NB)_2(Pyz)_2(H_2O)_2]$ (Table 3) are consistent with the corresponding ones in the reported structures. The simulated powder XRD diffraction pattern is shown in Fig. S2 which exhibits higher as well as lower intensities of reflections. The highest intensity is noticed at 2θ slightly greater than 5°.

3.2. Hirshfeld surface analysis

The field of crystal engineering is paying special attention to getting deep investigation of the intermolecular interactions in crystals as this is directly linked with the properties of crystals. In this regard, the study of intermolecular interactions is done by Hirshfeld surface analysis. Crystal Explorer v. 21.5[49] is used for that. For comparison, Hirshfeld surface analysis of $[Co(NB)_2(Pyz)_2(H_2O)_2]$ is compared with the analysis of the crystal structure with reference code DIFJUZ.[4] Hirshfeld surface idea emerged from making the fragments of the crystal density for integration. Hirshfeld surface designed on normalized distances separate contacts on the basis of interatomic contact type.[50–52] Short and long contacts are shown by red and blue spots on the surface whereas equal contacts (distance=sum of the Van der Waal radii) are shown by white spots. Figures 4(a) and 4(b) are Hirshfeld surfaces designed over normalized distances for $[Co(NB)_2(Pyz)_2(H_2O)_2]$ and DIFJUZ, respectively. For surface of $[Co(NB)_2(Pyz)_2(H_2O)_2]$, the red spots around amino H-atoms, carbonyl O-atom of pyrazine-carboxamide, H-atom of water and non-coordinating O-atom of benzoate indicate that these atoms form short contacts (Fig. 4(a)). Red spots on the surface of DIFJUZ around particular atoms indicate that these atoms formed short contacts (Fig. 4(b)). The O-atoms of nitro groups formed short contact in DIFJUZ whereas in case of $[Co(NB)_2(Pyz)_2(H_2O)_2]$, these atoms do not form any significant short contact. $\pi\cdots\pi$ stacking interactions can be checked and for that, the surface is formed on shape index. The regions marked in dashed elliptical shape on the surface for $[Co(NB)_2(Pyz)_2(H_2O)_2]$ and DIFJUZ (Figs. 4(c) and 4(d)) indicate that the rings are involved in $\pi\cdots\pi$ stacking interactions. 2D fingerprint plots enabled to find the contribution of individual contact in the stabilization of the supramolecular assembly.[53–55] In most of the

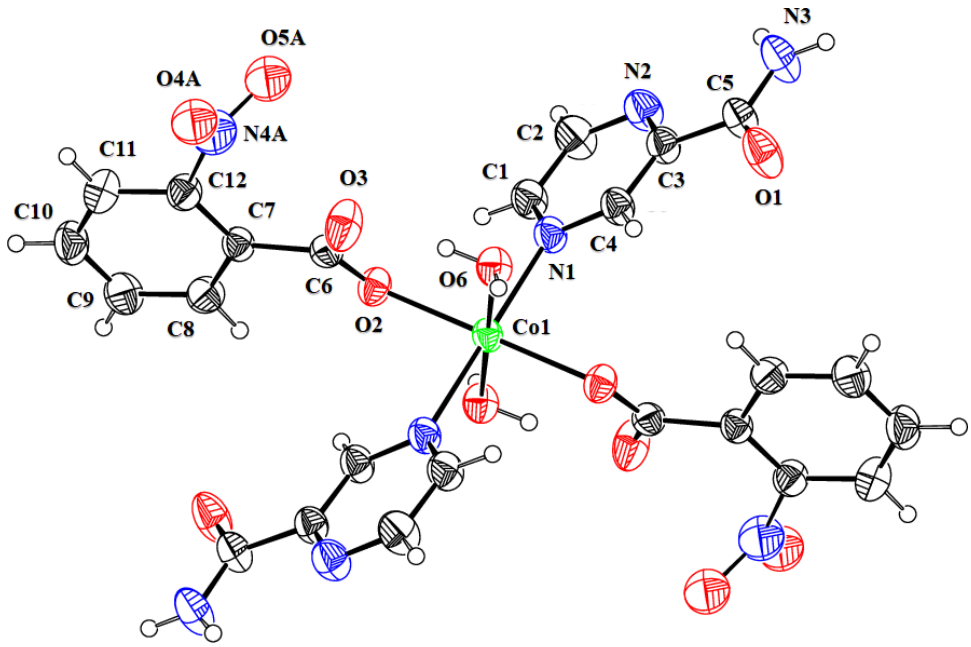

Fig. 2. (Color online) Molecular ORTEP view of $[Co(NB)_2(Pyz)_2(H_2O)_2]$ at 50% probability level.

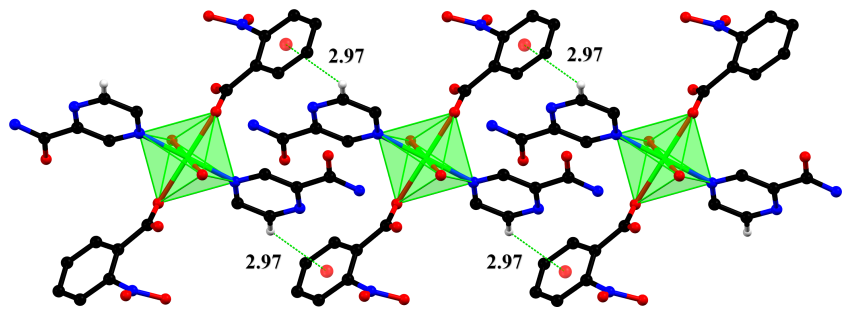

Fig. 3. (Color online) Graphical representation of C–H···π interactions view in $[Co(NB)_2(Pyz)_2(H_2O)_2]$. Distances are measured in Å.

Table 2. Hydrogen-bond geometry (Å, °) for $[Co(NB)_2(Pyz)_2(H_2O)_2]$.

D—H···*A*	*D*—H	H···*A*	*D*···*A*	<(*D*—H···*A*)°
O6—H6*A*···O1^{i}	0.79 (4)	2.10 (4)	2.881 (3)	167 (3)
O6—H6*B*···O3	0.85 (4)	1.77 (4)	2.595 (3)	163 (3)
N3—H3*A*···O1^{ii}	0.86	2.16	2.938 (3)	150
N3—H3*B*···O3^{iii}	0.86	2.29	2.986 (4)	138
***C*—H···π**	***C*—H**	**H···π**	***C*···π**	**<(*C*—H···π)°**
C2—H2···Cg1^{iii}	—	2.97	3.684 (3)	135

Notes: **Symmetry codes:** (i) $-x+1, -y, -z$; (iii) $x, y, z-1$; $-x+1, -y, -z-1$. Cg1 is the centroid of the phenyl ring.

Table 3. Geometry describing parameters of $[Co(NB)_2(Pyz)_2(H_2O)_2]$.

Bond lengths (Å)		Bond angles (°)	
Co1—O2	2.0843 (17)	O2^{i}—Co1—O2	180.0
Co1—O6	2.1278 (18)	O2—Co1—O6	93.51 (7)
Co1—N1	2.148 (2)	O2—Co1—O6^{i}	86.49 (7)
O1—C5	1.235 (3)	O6^{i}—Co1—O6	180.0
O2—C6	1.251 (3)	O2—Co1—N1	91.60 (8)
O3—C6	1.247 (3)	O2—Co1—N1^{i}	88.40 (8)
N1—C1	1.328 (3)	O6—Co1—N1	86.28 (8)
N1—C4	1.337 (3)	O6—Co1—N1^{i}	93.72 (8)
N2—C2	1.328 (4)	N1^{i}—Co1—N1	180.0

Notes: **Symmetry code**: (i) $-x, -y, -z$.

DOI: 10.1142/S2737416524500455

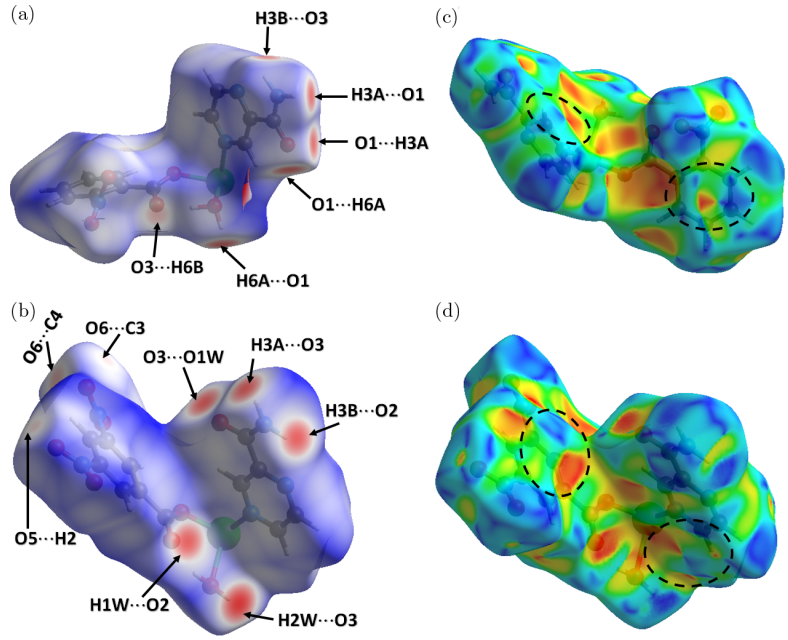

Fig. 4. (Color online) Hirshfeld surface designed by using (a),(b) normalized distances, (c),(d) shape index for $[Co(NB)_2(Pyz)_2(H_2O)_2]$ and crystal structure with reference code DIFJUZ.

crystals, H···H contact dominant on other contacts but in case of $[Co(NB)_2(Pyz)_2(H_2O)_2]$ and DIFJUZ, H···O contact is the most important one as it has highest contribution (36.3%) in $[Co(NB)_2(Pyz)_2(H_2O)_2]$ (Fig. 5(a)) and 41.4% in DIFJUZ (Fig. 5(d)). The contacts at second and third numbers are H···H and H···C in $[Co(NB)_2(Pyz)_2(H_2O)_2]$ but in case of DIFJUZ, the third larger contributor is C···O contact. The contribution of H···H contact is 9.6% larger in case of $[Co(NB)_2(Pyz)_2(H_2O)_2]$ as compared to in DIFJUZ. The 2D fingerprint plots for the other interatomic contacts are shown in Figs. S3 and S4, respectively. Enrichment ratios provide the pairs of atoms that have a higher propensity to form contacts than other pairs.[56] The pair with an enrichment ratio greater than one has higher tendency to form crystal packing interactions than others. Carbon-nitrogen pair has the highest such propensity with enrichment ratio of 3.59 and 1.84 in $[Co(NB)_2(Pyz)_2(H_2O)_2]$ and DIFJUZ, respectively (Table S1). After that, the pair of higher propensity is oxygen-cobalt with an enrichment ratio of 2.08 in $[Co(NB)_2(Pyz)_2(H_2O)_2]$ whereas the carbon-carbon pair with enrichment ratio 1.61 for DIFJUZ.

3.3. Voids analysis

The empty spaces generated by the packing of molecules that are not solvent-accessible provide information about the response of the crystal upon external stress. Such empty spaces or voids are calculated based on the idea of pro-crystal electron density.[57] Figure 6 shows isosurfaces of voids in $[Co(NB)_2(Pyz)_2(H_2O)_2]$ and DIFJUZ. The volume of voids is 160.60 and 109.14 Å^3 in $[Co(NB)_2(Pyz)_2(H_2O)_2]$ and DIFJUZ, respectively. The voids space is 11.4% and 14.2% voids in $[Co(NB)_2(Pyz)_2(H_2O)_2]$ and DIFJUZ, respectively. Majority of the spaces in supramolecular assembly are occupied by molecules indicating the absence of any large cavity and both compounds are expected to bear a considerable amount of stress without permanent change in their shapes.

3.4. Interaction energies between molecular pairs

The supramolecular assembly investigation is further carried out by intermolecular interaction energies calculations at B3LYP/6-31G(d,p) electron density model using Crystal Explorer version 21.5.[49] Generation of a 3.8 Å cluster around the reference molecule is added in calculations. The interaction between molecules is the sum of electrostatic coulomb, dispersion, polarization and repulsion energy.[58] The later energy type is always repulsive (positive value) whereas second and third are always attractive (negative value). The Coulomb energy between a pair can be attractive or repulsive but in the

DOI: 10.1142/S2737416524500455
J. Comput. Biophys. Chem. **2024**, *23*(10), 1325–1338

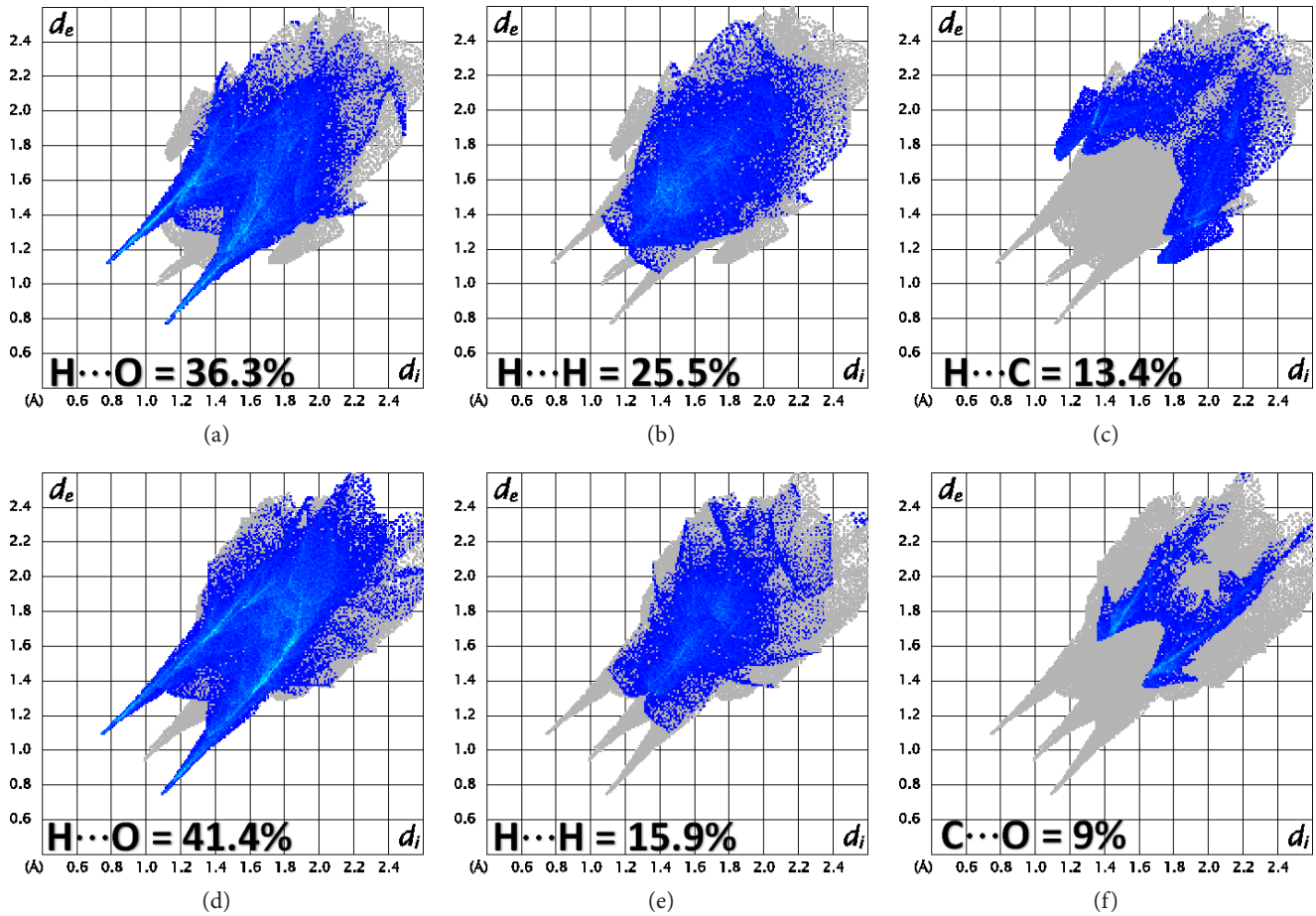

Fig. 5. (Color online) 2D fingerprint plots for important interatomic contacts for (a)–(c) $[Co(NB)_2(Pyz)_2(H_2O)_2]$, (d)–(f) DIFJUZ.

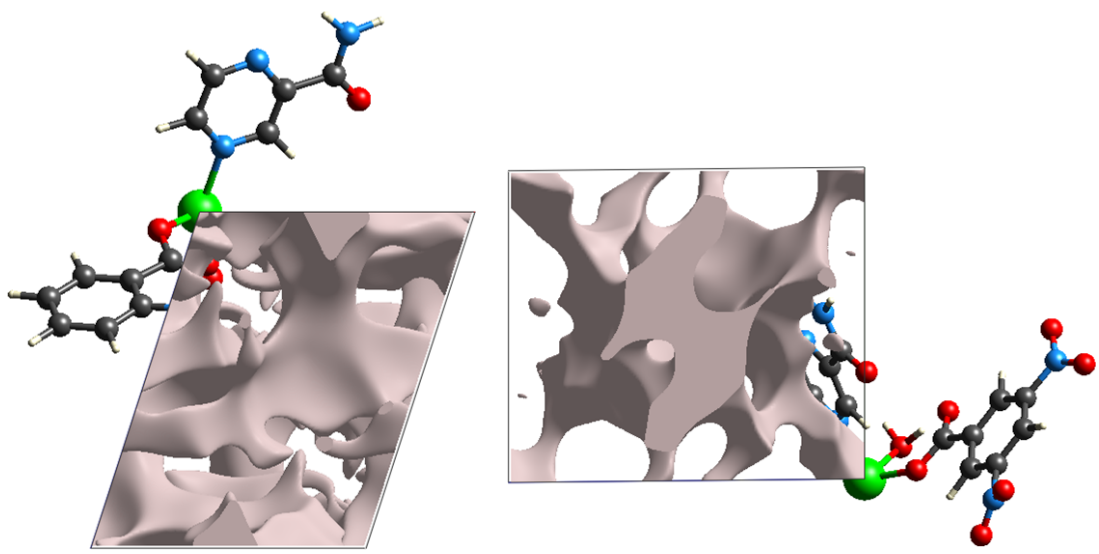

Fig. 6. (Color online) Isosurfaces of voids for (a) $[Co(NB)_2(Pyz)_2(H_2O)_2]$ and (b) DIFJUZ.

DOI: 10.1142/S2737416524500455
J. Comput. Biophys. Chem. **2024**, *23* (10), 1325–1338

	N	Symop	R	E_ele	E_pol	E_dis	E_rep	E_tot	E_att	%E_att		
										E_ele	E_pol	E_dis
	2	x, y, z	9.93	-35.4	-13.1	-75.5	55	-78.9	-124.0	28.5	10.6	60.9
	4	-x+1/2, y+1/2, -z+1/2	10.98	-9.7	-7.3	-26	16.4	-28.2	-43.0	22.6	17.0	60.5
	2	x, y, z	7.74	-83.7	-24.7	-59.1	84.8	-105.9	-167.5	50.0	14.7	35.3
	4	-x+1/2, y+1/2, -z+1/2	12.01	-4.6	-7	-29.3	10.6	-29	-40.9	11.2	17.1	71.6
	2	x, y, z	14.34	-48.6	-11.9	-19.5	48.6	-47.2	-80.0	60.8	14.9	24.4

(a)

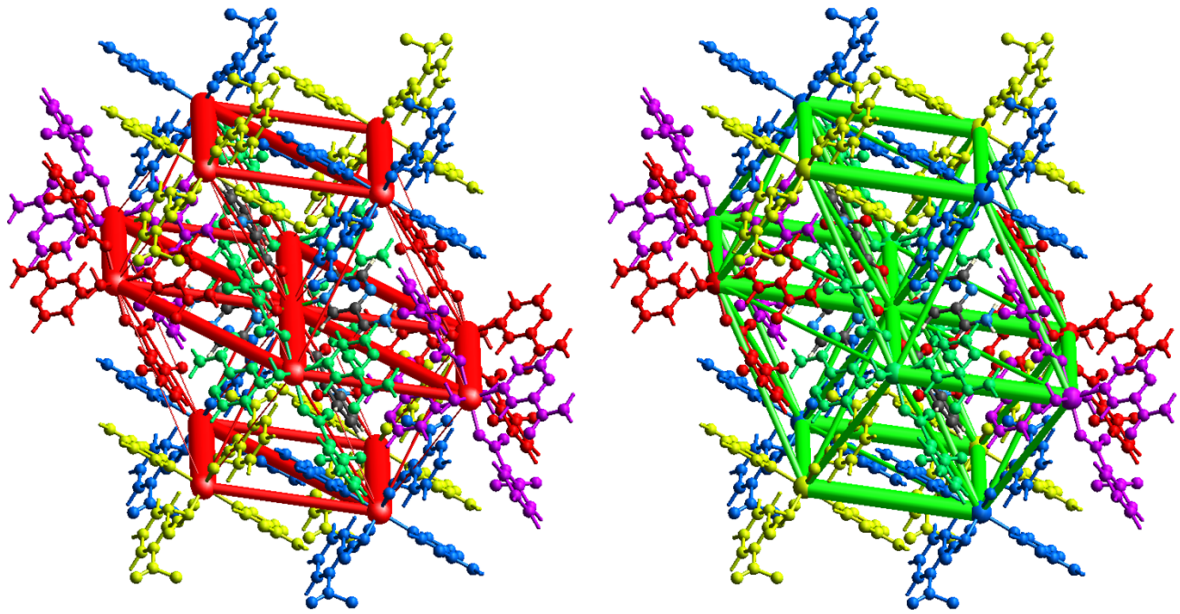

(b) (c)

Fig. 7. **(Color online)** (a) Interaction energy results in detail, energy frameworks for (b) coulomb energy and (c) dispersion energy.

present case, it is attractive for the pairs involved in calculations (Fig. 7(a)). Total interaction energy and contribution of total attractive energy are greatest for the pair with the smallest intermolecular separation although the dispersion energy is greatest for the pair which has the second smallest separation. The contribution of coulomb, dispersion and polarization energies in total attractive energy is also calculated for the pairs which showed that the dispersion energy has a prominent role in attractive energy contribution as compared to others. Furthermore, difference of the role of coulomb and dispersion energy is displayed by energy frameworks in which the center of molecules is joined by the cylinder of width proportional to the strength of the corresponding energy type. Although the width of cylinders for the larger contribution pairs looks almost identical and the width of the central cylinder is larger for Coulomb energy (Fig. 7(b)) than dispersion energy, there are lots of other pairs for which the width of cylinders for Coulomb energy is also negligible as compared to the corresponding width for dispersion energy (Fig. 7(c)). This showed that the dispersion energy played the most dominant role in the stabilization of the supramolecular assembly as compared to Coulomb energy.

3.5. Computational study

To thoroughly understand the title compound, we performed the Density Functional Theory (DFT) computational analysis. The optimized geometry is illustrated in Fig. 8. The values of geometry parameters acquired from XRD are consistent with the corresponding ones calculated by DFT. Through an analysis of the energy levels of the highest occupied molecular orbital (HOMO) and the lowest unoccupied molecular orbital (LUMO), we gained valuable insights into the compound's energy distribution and anticipated chemical

DOI: 10.1142/S2737416524500455
J. Comput. Biophys. Chem. **2024**, *23*(10), 1325–1338

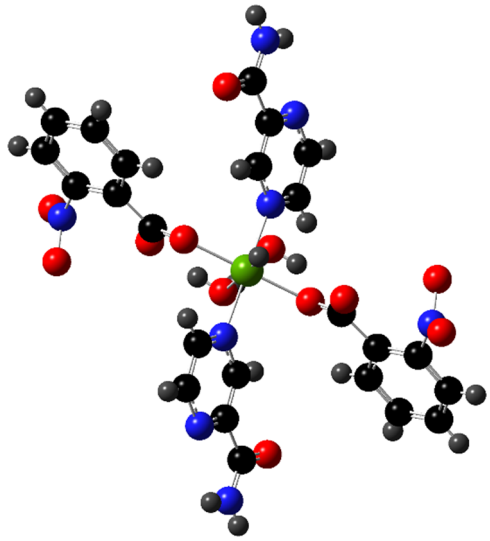

Fig. 8. (color online) Optimized geometry of $[Co(NB)_2(Pyz)_2(H_2O)_2]$.

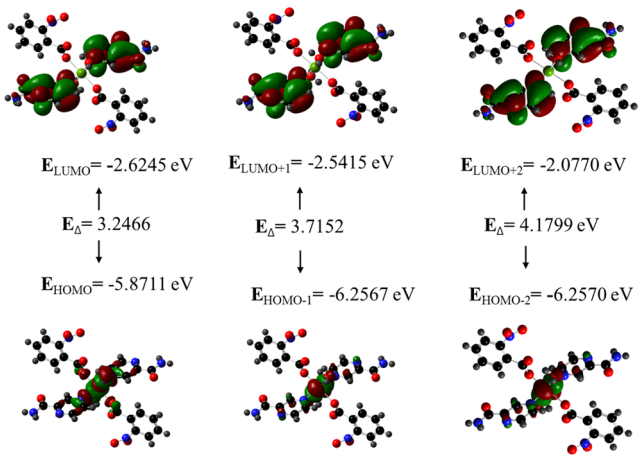

Fig. 9. (Color online) Molecular orbitals of the $[Co(NB)_2(Pyz)_2(H_2O)_2]$ for experimental data.

behavior.[59–61] We visualized the molecular orbitals (Fig. 9), where the red color represents the positive phase, while the negative phase is depicted in green. The energy difference between the HOMO and LUMO elucidates the charge transfer interaction occurring within the molecule.[62] The negativity of both E_{HOMO} and E_{LUMO} signifies the compound's stability. Furthermore, the energy gap ΔE ($E_{LUMO} - E_{HOMO}$) denotes the minimum energy needed for electron excitation within the compound. This gap plays a critical role in determining the compound's kinetic stability and chemical reactivity.[63–65] A compound possessing a relatively large energy difference of HOMO–LUMO is considered hard, displaying lower polarizability and reactivity. Conversely, compounds with a narrower HOMO–LUMO gap are characterized as soft, exhibiting higher polarizability and reactivity. This understanding aids in elucidating the compound's behavior and potential applications. We evaluated the energy levels spanning from (HOMO) to the third HOMO (HOMO-2), as well as from (LUMO) to the third LUMO (LUMO+2). Detailed energy values for these molecular orbitals can be found in Table 4, accompanied by visual representations in Fig. 9.

Data of the calculated energy for HOMO-HOMO-2 and LUMO-LUMO+2 and energy differences between them (see Table 4). The HOMO-LUMO value of −3.2466 eV suggests a moderate energy difference between the (HOMO) and (LUMO). This implies that the molecule may possess a moderate level of stability. While not as wide as larger HOMO-LUMO gaps, a moderate gap indicates that the molecule still has the potential for reactivity. It may undergo electron excitation more readily compared to molecules with larger HOMO-LUMO gaps, making it somewhat reactive.

Also, the chemical reactivity parameters of the molecule under this study, including its chemical softness (S), hardness (η), chemical potential (μ) and electrophilicity index (ω), were found to be 0.308015 eV^{-1}, 1.62, 4.25, 5.56 eV, respectively. Electrophilicity value of 5.56 eV indicates a relatively high electrophilic reactivity, which means that $[Co(NB)_2(Pyz)_2(H_2O)_2]$ is highly reactive towards electrophiles, which are species that seek electrons to form bonds. Molecules with high electrophilicity indices are more likely to encounter reactions where they act as electron acceptors.

Table 4. Energy data for the HOMO, HOMO-2, LUMO and LUMO+2, along with the energy differences among these orbitals.

Experimental geometry				
Level	Energy (eV)	Level	Energy (eV)	ΔEnergy (eV)
HOMO	−5.8711	LUMO	−2.6245	−3.2466
HOMO	−5.8711	LUMO+1	−2.5415	−3.3296
HOMO	−5.8711	LUMO+2	−2.0770	−3.7941
HOMO-1	−6.2567	LUMO	−2.6245	−3.6322
HOMO-2	−6.2570	LUMO	−2.6245	−3.6324
HOMO-1	−6.2567	LUMO+1	−2.5415	−3.7152
HOMO-2	−6.2570	LUMO+2	−2.0770	−4.1799

DOI: 10.1142/S2737416524500455
J. Comput. Biophys. Chem. **2024**, *23* (10), 1325–1338

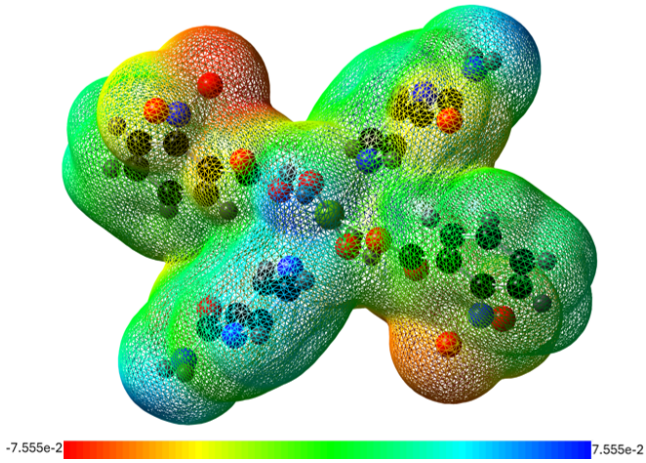

Fig. 10. (Color online) The molecular electrostatic potential plot of the title compound.

3.5.1. *Molecular electrostatic potential analysis*

The Molecular Electrostatic Potential (MEP) analysis is a valuable tool for identifying regions in molecules that are prone to nucleophilic or electrophilic attacks.[63–65] This method is based on the distribution of positive and negative charges within the molecular structure. In the experimental model (see Fig. 10), the MEP values range from −7.555*e*−2 to +7.555*e*−2.

Areas with negative electrostatic potential are more likely to attract nucleophiles, while those with positive potential are more likely to attract electrophiles. The analysis reveals that the nitro group (R-NO2) in the molecule shows strong electrophilic properties, while the amino group demonstrates nucleophilic behavior in the positively charged regions.

4. CONCLUSIONS

The cobalt complex was synthesized by two-nitrobenzoic acid and pyrazine-two-carboxamide ligands assisted by hot water, sodium bicarbonate and cobalt acetate tetrahydrate. The crystal structure of the cobalt complex was verified by single crystal XRD technique which showed that the complex was mononuclear and ligands were coordinated in such a way that the octahedral geometry was formed. Supramolecular assembly was stabilized by O–H···O and N–H···N, $\pi\cdots\pi$ and C–H···π interactions. Hirshfeld surface analysis inferred that most of the contribution for supramolecular assembly was from O···H contact followed by H···H and H···C contacts. Enrichment ratios showed that carbon-nitrogen pair had the highest tendency to make crystal-packing interactions. Void analysis predicted that the crystal could bear considerable amount of stress. Interaction energy calculations showed that dispersion energy was the one that played the most significant role in stabilization for the supramolecular assembly. The computational analysis using DFT consistently matched the geometry parameters found in the experimental XRD data, indicating the molecule's stability. A moderate HOMO-LUMO energy gap suggests potential reactivity, while a high electrophilicity index highlights its tendency for electron-accepting reactions. Additionally, the analysis of the molecular electrostatic potential shows that the experimental geometry of the organic salt exhibits both electronegative and electropositive regions, enabling nucleophilic and electrophilic attacks, thus indicating high chemical reactivity.

ACKNOWLEDGMENTS

The authors are grateful to the Researchers Supporting Project Number (RSP2024R273), King Saud University, Riyadh, Saudi Arabia, for providing funding support. The authors are also grateful to New Mexico Highlands University, Las Vegas, New, Mexico, 87701 USA for DFT study with Grant No. (NSF DMR-2122108 (PREM)).

STATEMENT OF USAGE OF ARTIFICIAL INTELLIGENCE

I confirm that ChatGPT was not used in the preparation of the paper.

DATA AVAILABILITY

CCDC number 2102866 contains the supplementary crystallographic data for the compound. The data can be obtained free of charge via http://www.ccdc.cam.ac.uk/conts/retrieving.html, or from the Cambridge Crystallographic Data Centre, 12 Union Road, Cambridge CB2 1EZ, UK; fax: (+44) 1223-336-033; or e-mail: deposit@ccdc.cam.ac.uk.

AUTHOR CONTRIBUTIONS

Melike Nur Deniz: Synthesis and helped in characterization. **Muhammad Ashfaq:** Write up introduction, Single Crystal X-rays diffraction, Hirshfeld surface analysis, interaction energies calculations parts of manuscript. **Seyhan Ozturk**: Synthesis. **Necmi Dege**: Performed single crystal XRD. **Novikov Egor:** Performed DFT calculations. **Muhammad Nawaz**

Tahir: single crystal XRD data refinement. **Naila Guliyeva:** refinement of manuscript. **Mohammad Shahidul Islam** and **Tahani Mazyad Almutairi:** helped in funding of the project and refinement of manuscript. **Suraj N. Mali:** helped in charaetirazation and overall refinement of the paper.

CONFLICT OF INTEREST

The authors declare no competing financial interests or personal relationships that could have appeared to influence the work reported in this paper.

FUNDING INFORMATION

Authors are grateful to the Researchers Supporting Project Number (RSP2024R273), King Saud University, Riyadh, Saudi Arabia, for providing funding support.

SUPPLEMENTARY INFORMATION

The Supplementary Information are available at: https://www.worldscientific.com/doi/suppl/10.1142/S2737416524500455.

ORCID

Melike Nur Deniz
https://orcid.org/0009-0004-0846-6574
Muhammad Ashfaq
https://orcid.org/0000-0001-6663-8777
Seyhan Ozturk
https://orcid.org/0000-0003-4638-5578
Egor Novikov
https://orcid.org/0009-0009-3055-3881
Muhammad Nawaz Tahir
https://orcid.org/0000-0002-6815-9806
Saltanat Arshad Aghayeva
https://orcid.org/0000-0001-6982-7215
Mohammad Shahidul Islam
https://orcid.org/0000-0002-4612-5875
Necmi Dege
https://orcid.org/0000-0003-0660-4721
Tahani Mazyad Almutairi
https://orcid.org/0000-0002-0987-6303
Suraj N. Mali
https://orcid.org/0000-0003-1995-136X

References

1. Yambulatov, D. S. *et al.* Synthesis, Structure, Biological Activity, and Luminescence Properties of a "Butterfly"-Type Silver Cluster with 3-Benzyl-4-phenyl-1,2,4-triazol-5-thiol. *Molecules* **2024**, *29*(1) 12227–12234. https://doi.org/10.3390/molecules29010105.
2. Damena, T.; Zeleke, D.; Desalegn, T.; Demissie, T. B.; Eswaramoorthy, R. Synthesis, Characterization, and Biological Activities of Novel Vanadium(IV) and Cobalt(II) Complexes. *ACS Omega* **2022**, *7* (5), 4389–4404. https://doi.org/10.1021/acsomega.1c06205.
3. Chang, E. L.; Simmers, C.; Knight, D. A. Cobalt Complexes as Antiviral and Antibacterial Agents. *Pharmaceuticals* **2010**, *3* (6), 1711–1728. https://doi.org/10.3390/ph3061711.
4. Vasková, Z.; Padělková, Z.; Mazur, M.; Valigura, D.; Moncol, J. Synthesis, Properties and Crystal Structures of Nitrobenzoatocopper(II) Complexes with Pyrazinecarboxamide. *Transit. Met. Chem.* **2011**, *36* (8), 883–889. https://doi.org/10.1007/s11243-011-9545-4.
5. A. S. Goher, M.; A. Mautner, F. A Novel Polymeric Copper(I) Complex with an Unusual Azide Bridge. Synthesis and Crystal Structure of $[Cu(pyza)(\mu\text{-}1,1,3\text{-}N_3)]_\infty$ (pyza = pyrazinecarboxamide). *J. Chem. Soc., Dalton Trans.* **1999**, (10), 1535–1536. https://doi.org/10.1039/A901425J.
6. Mir Mohammad Sadegh, B.; Azhdari Tehrani, A.; Khavasi, H. R. catena-Poly[[bis(pyrazine-2-carboxamide-κN^4) mercury (II)]-di-μ-bromido]. *Acta Crystallogr., Sect. E: Struct. Rep. Online* **2010**, *66* (2), m158–m158. https://doi.org/10.1107/S1600536810001182.
7. Çelik, Y.; Bozkurt, E.; Karabulut, B.; Dege, N. Crystal Structure and EPR Investigation of Pyrazinamide Containing Copper (II) 2-Nitrobenzoate Single Crystal. *Acta Phys. Pol. A* **2016**, *130* (1), 163–166. https://doi.org/10.12693/APhysPolA.130.163.
8. Tanase, S.; Evangelisti, M.; de Jongh, L. J.; Smits, J. M. M.; de Gelder, R. Crystal Structure, Magnetic and Thermal Properties of the One-Dimensional Complex $[Nd(pzam)_3(H_2O)Mo(CN)_8]\cdot H_2O$. *Inorganica Chim. Acta.* **2008**, *361* (12), 3548–3554. https://doi.org/10.1016/j.ica.2008.03.026.
9. Lawal, M.; Obaleye, J. A.; Jadeja, R. N.; Gupta, V. K.; Nnabuike, G. G.; Bamigboye, M. O.; Roy, H.; Yusuff, O. K.; Raji, A. T. Mixed Pyrazinamide and 4-Dimethylaminopyridine Nickel(II) Complex: Characterization, DFT, and Biological Potentials. *J. Mol. Struct.* **2024**, *1300*, 137171. https://doi.org/10.1016/j.molstruc.2023.137171.
10. Yoshida, M.; Shimada, T.; Ishida, T.; Kogane, T. Crystal Structures and Magnetic Properties of Two-Dimensional Copper(II) Complexes Bridged with Pyrazine-2-Carboxamide. *Polyhedron* **2013**, *66*, 75–80. https://doi.org/10.1016/j.poly.2013.02.033.
11. Munakata, M.; Wu, L. P.; Kuroda-Sowa, T.; Maekawa, M.; Moriwaki, K.; Kitagawa, S. Two Types of New Polymeric

Copper(I) Complexes of Pyrazinecarboxamide Having Channel and Helical Structures. *Inorg. Chem.* **1997**, *36* (23), 5416–5418. https://doi.org/10.1021/ic970427f.

12. Tanase, S.; Gallego, P. M.; Bouwman, E.; de Gelder, R.; Reedijk, J. A New Polymeric Copper(II) Complex Containing Pyrazine-2-Carboxyamide (pzca): Synthesis and Crystal Structure of $\{[Cu(pzca)(CH_3CN)_3](ClO_4)_2 \cdot H_2O\}_n$. *Inorg. Chem. Commun.* **2005**, *8* (8), 680–683. https://doi.org/10.1016/j.inoche.2005.05.004.
13. Groom, C. R.; Bruno, I. J.; Lightfoot, M. P.; Ward, S. C. The Cambridge Structural Database. *Acta Crystallogr. Sect. B: Struct. Sci., Cryst. Eng. Mater.* **2016**, *72* (2), 171–179. https://doi.org/10.1107/S2052520616003954.
14. Chisca, D.; Siminel, A. V.; Fonari, M. S.; Croitor, L. Structural Characterization and Emission Properties of Mixed-ligand Transition Metal Coordination Complexes with Dicarboxylic Acids and Pyrazinecarboxamide. *Polyhedron* **2019**, *170*, 245–252. https://doi.org/10.1016/j.poly.2019.05.052.
15. Prananto, Y. P. Coordination Polymer of M(II)-Pyrazinamide (M = Co, Cd) with Double End-to-End Thiocyanate Bridge. *IOP Conf. Ser.: Mater. Sci. Eng.* **2018**, *299* (1), 012032. https://doi.org/10.1088/1757-899X/299/1/012032.
16. Ahmad, M. S.; Khalid, M.; Khan, M. S.; Shahid, M.; Ahmad, M. Exploiting One Dimensional Polymer for Environmental Monitoring: Co based Coordination Polymer for Efficient Removal of Cationic Dyes. *J. Solid State Chem.* **2022**, *313*, 123307. https://doi.org/10.1016/j.jssc.2022.123307.
17. Somasundaram, J. D.; Ebrahimi, A.; Nandan, S. P.; Cherevan, A.; Eder, D.; Šupolíková, M.; Nováková, E.; Gyepes, R.; Krivosudský, L. Functionalization of Decavanadate Anion by Coordination to Cobalt(II): Binding to Proteins, Cytotoxicity, and Water Oxidation Catalysis. *J. Inorg. Biochem.* **2023**, *239*, 112067. https://doi.org/10.1016/j.jinorgbio.2022.112067.
18. Pannu, A. P. S.; Lee, S.; Lee, Y. Diaquabis (Pyrazine-2-Carboxamide-κ2N1, O) Cobalt (II) Dinitrate. *Acta Crystallogr. Sect. E: Struct. Rep. Online* **2012**, *68* (4), m512–m513. https://doi.org/10.1107/S1600536812012573.
19. Tenhunen, A. Studies on Metal Complexes of Pyrazine and Itse Derivatives. Part 1, Unit Cell and Other Properties of Pyrazine(II) Sulfate Hexahydrate. *Suomen kemistilehti B* **1970**, *40*, 105–108.
20. Farag, A. A.; Ali, T. A. The Enhancing of 2-Pyrazinecarboxamide Inhibition Effect on the Acid Corrosion of Carbon Steel in Presence of Iodide Ions. *J. Ind. Eng. Chem.* **2015**, *21*, 627–634. https://doi.org/10.1016/j.jiec.2014.03.030.
21. Dolezal, M.; Cmedlova, P.; Palek, L.; Vinsova, J.; Kunes, J.; Buchta, V.; Jampilek, J.; Kralova, K. Synthesis and Antimycobacterial Evaluation of Substituted Pyrazinecarboxamides. *Eur. J. Med. Chem.* **2008**, *43* (5), 1105–1113. https://doi.org/10.1016/j.ejmech.2007.07.013.
22. Romero, A. H. *et al*. Tautomerism and Rotamerism of Favipiravir and Halogenated Analogues in Solution and in the Solid State. *J. Org. Chem.* **2023**, *88* (15), 10735–10752. https://doi.org/10.1021/acs.joc.3c00777.
23. Cui, Z.-W.; Lin, H.-Y.; Xu, N.; Chang, Z.-H.; Wang, X.; Liu, G.-C.; Wang, X.-L. Two Polyoxometalate-Based Cuii Complexes with a New Semi-Rigid Bis(Pyrazine)-Bis(Amide) Ligand: Architectures, Adsorption Activities for Dyes and Bifunctional Electrocatalytic Performances. *Inorg. Chem. Commun.* **2020**, *122*, 108285. https://doi.org/10.1016/j.inoche.2020.108285.
24. Poreddy, A. R.; Neumann, W. L.; Freskos, J. N.; Rajagopalan, R.; Asmelash, B.; Gaston, K. R.; Fitch, R. M.; Galen, K. P.; Shieh, J.-J.; Dorshow, R. B. Exogenous Fluorescent Tracer Agents Based on Pegylated Pyrazine Dyes for Real-Time Point-of-Care Measurement of Glomerular Filtration Rate. *Bioorg. Med. Chem.* **2012**, *20* (8), 2490–2497. https://doi.org/10.1016/j.bmc.2012.03.015.
25. Sathya Priyadarshini, G.; Selvi, G. Luminescence Cobalt (II) Complexes: Synthesis, Characterization, Photophysical and DFT Study. *Mater. Today: Proc.* **2021**, *40*, S19–S27. https://doi.org/10.1016/j.matpr.2020.03.252.
26. Nagaveni, V. B.; Mahadevan, K. M.; Vijayakumar, G. R.; Nagabhushana, H.; Naveen, S.; Lokanath, N. K. Synthesis, crystal Structure and Excellent Photoluminescence Properties of Copper (II) and Cobalt (II) Complexes with Bis(1[(4-butylphenyl)imino]Methyl Naphthalen-2-ol) Schiff Base. *J. Sci.: Adv. Mater. Devices* **2018**, *3* (1), 51–58. https://doi.org/10.1016/j.jsamd.2018.01.001.
27. Gönül, İ.; Fakı, E.; Ay, B.; Köse, M.; Serin, S. Cobalt(II), Nickel(II) and Copper(II) Complexes of a Schiff Base ligand: Synthesis, Structural Characterization and Luminescence Properties. *Transit. Met. Chem.* **2018**, *43* (1), 73–81. https://doi.org/10.1007/s11243-017-0195-z.
28. Wang, Z.-H.; Chen, S.-F.; Wang, D.-F.; Hao, H.-J.; Mei, H.-X.; Huang, R.-B.; Zheng, L.-S. Syntheses, Structures, and Photoluminescent Properties of Two Silver (I) Coordination Polymers with 1, 4-Bis(Imidazol-1-Ylmethyl) Benzene. *J. Mol. Struct.* **2013**, *1050*, 97–102. https://doi.org/10.1016/j.molstruc.2013.07.004.
29. Zhang, T.; Huang, H.-Q.; Mei, H.-X.; Wang, D.-F.; Wang, X.-X.; Huang, R.-B.; Zheng, L.-S. New Silver(I) Coordination Polymers Constructed from Pyrazine Derivatives and Aromatic Carboxylic Acids: Syntheses,

Structures and Photoluminescence. *J. Mol. Struct.* **2015**, *1100*, 237–244. https://doi.org/10.1016/j.molstruc.2015.07.048.

30. Bozkurt, E.; Çelik, Y.; Çöpür, F.; Dege, N.; Topcu, Y.; Karabulut, B. Synthesis, Crystal Structure and EPR Studies of Vanadyl Doped $[Co(2\text{-}nbH)_2(ina)_2(H_2O)]$ Complex. *Chem. Phys. Lett.* **2016**, *659*, 186–191. https://doi.org/10.1016/j.cplett.2016.07.024.
31. Stachová, P.; Valigura, D.; Koman, M.; Melník, M.; Korabik, M.; Mroziński, J.; Glowiak, T. Crystal Structure, Magnetic and Spectral Properties of Tetrakis(2-Nitrobenzoato)di(Aqua)dicopper(II) Dihydrate. *Polyhedron* **2004**, *23* (8), 1303–1308. https://doi.org/10.1016/j.poly.2003.12.025.
32. Kathiresan, A.; Srinivasan, K.; Brinda, S.; Nethaji, M.; Govindarajan, S. Synthesis and Characterization of Cobalt(II), Nickel(II), Copper(II) and Zinc(II) Complexes of 2-Nitrobenzoic Acid with Methyl Carbazate as Ancillary Ligand. Crystal Structure of the Copper(II) Complex. *Transit. Met. Chem.* **2012**, *37* (4), 393–397. https://doi.org/10.1007/s11243-012-9601-8.
33. Yang, Y. Y.; Zhou, L.-X.; Zheng, Y. Q.; Zhu, H.-L.; Li, W.-Y. Hydrothermal Synthesis, Photoluminescence and Photocatalytic Properties of Two Silver(I) complexes. *J. Solid State Chem.* **2017**, *253*, 211–218. https://doi.org/10.1016/j.jssc.2017.05.009.
34. Yang, Y.-Y.; Zhou, L.-X.; Zhu, H.-L.; Li, W.-Y.; Zheng, Y.-Q. Synthesis, Crystal Structures and Photocatalytic Properties of Four Silver(I) Coordination Polymers Based on Nitroterephthalic Acid. *Polyhedron* **2018**, *148*, 161–170. https://doi.org/10.1016/j.poly.2018.04.009.
35. Kar, P.; Ida, Y.; Kanetomo, T.; Drew, M. G. B.; Ishida, T.; Ghosh, A. Synthesis of Mixed-valence Hexanuclear Mn(ii/iii) Clusters from its Mn(ii) Precursor: Variations of Catecholase-like Activity and Magnetic Coupling. *Dalton Trans.* **2015**, *44* (21), 9795–9804. DOI:10.1039/C5DT00709G.
36. Wang, C.; Xu, W.; Ren, Y.-N.; Zhu, H.-L.; Zheng, Y.-Q. Removal of Tetracycline Hydrochloride from Aqueous Solution by Three 3D Uranyl-organic Frameworks. *Inorganica Chim. Acta.* **2019**, *493*, 29–37. https://doi.org/10.1016/j.ica.2019.04.046.
37. Yang, Y.-Y.; Zhou, L.-X.; Zheng, Y.-Q.; Zhu, H.-L. Four New Silver-Based Complexes Constructed from 3-Nitrophthalic Acid and Pyrazine-Like Ligands: Syntheses, Crystal Structures and Photodegradation Activities. *Polyhedron* **2017**, *134*, 345–355. https://doi.org/10.1016/j.poly.2017.06.028.
38. Amani, A.; Derikvand, Z.; Dusek, M.; Eigner, V.; Azadbakht, A. A New One-Dimensional 3D Supramolecular Coordination Polymer of CdII Based on Pyrazine and 3-Nitropthphthalic Acid: Synthesis, Characterization, Crystal Structure, Thermal Analysis. *Inorg. Nano-Met. Chem.* **2018**, *48* (1), 74–79. https://doi.org/10.1080/24701556.2017.1357634.
39. Askerov *et al*. Synthesis, Crystal Structure, Exploration of the Supramolecular Assembly through Hirshfeld Surface Analysis and Bactericidal Activity of the Cadmium Organometallic Complexes obtained from the Heterocyclic Ligand. *Results Chem.* **2022**, *4*, 100600. https://doi.org/10.1016/j.rechem.2022.100600.
40. Ali, U. S.; Siddiqui, W. A.; Ashraf, A.; Raza, M. A.; Batoo, K. M.; Imran, M.; Shirsath, S. E.; Ashfaq, M.; Tahir, M. N.; Niaz, S. Structure Elucidation {single X-ray Crystal Diffraction Studies, Hirshfeld Surface Analysis, DFT} and Antibacterial Studies of 1,2-Benzothiazine Metal Complexes. *J. Mol. Struct.* **2024**, *1306*, 137824. https://doi.org/10.1016/j.molstruc.2024.137824.
41. Khan, M. E. I.; Ashfaq, M.; Tahir, M. N.; Munawar, K. S.; Ayub, K.; Nawaz, F.; Yar, M.; Husnain, K. Synthesis, Characterization, Single Crystal XRD, Solid State Assembly Inspection by Hirshfeld Surface Analysis, and Theoretical Studies of Pb(II) complex with Thiourea Derivative. *J. Mol. Struct.* **2024**, *1304*, 137689. https://doi.org/10.1016/j.molstruc.2024.137689.
42. Kargar, H. *et al*. Structural and Electrochemical Properties of a Cu(I) Schiff-Base Complex: Catalytic Application to the Synthesis of Tetrahydropyrimidine Derivatives. *Inorganica Chim. Acta*. **2024**, *570*, 122160. https://doi.org/10.1016/j.ica.2024.122160.
43. Sheldrick, G. M. SHELXT–Integrated Space-Group and Crystal-Structure Determination. *Acta Crystallogr., Sect. A: Found. Adv.* **2015**, *71* (1), 3–8. https://doi.org/10.1107/S2053273314026370.
44. Sheldrick, G. M. Crystal Structure Refinement with SHELXL. *Acta Crystallogr. C Struct. Chem.* **2015**, *71* (1), 3-8. https://doi.org/10.1107/S2053229614024218.
45. Spek, A. L. Structure Validation in Chemical Crystallography. *Acta Crystallogr. D Biol. Crystallogr.* **2009**, *65* (2), 148–155. https://doi.org/10.1107/S090744490804362X.
46. Macrae, C. F.; Sovago, I.; Cottrell, S. J.; Galek, P. T.; McCabe, P.; Pidcock, E.; Platings, M.; Shields, G. P.; Stevens, J. S.; Towler, M. Mercury 4.0: From Visualization to Analysis, Design and Prediction. *J. Appl. Crystallogr.* **2020**, *53* (1), 226–235. https://doi.org/10.1107/S1600576719014092.
47. Frisch, M. J. *et al*. Gaussian 16 Revision. C.01. 2016.
48. Dennington, R.; Keith, T. A.; Millam, J. M. GaussView 6.0. 16. Semichem Inc.: Shawnee Mission, KS, USA, 2016.
49. Spackman, P. R.; Turner, M. J.; McKinnon, J. J.; Wolff, S. K.; Grimwood, D. J.; Jayatilaka, D.; Spackman, M. A.

CrystalExplorer: A Program for Hirshfeld Surface Analysis, Visualization and Quantitative Analysis of Molecular Crystals. *J. Appl. Crystallogr.* **2021**, *54* (3), 1006–1011. https://doi.org/10.1107/S1600576721002910.

50. Spackman, M. A.; Jayatilaka, D. Hirshfeld Surface Analysis. *Cryst. Eng. Comm.* **2009**, *11* (1), 19–32. https://doi.org/10.1039/B818330A.
51. Malik, A. N.; Ali, A.; Ashfaq, M.; Tahir, M. N.; Alam, M. M.; Mostafa, M. S.; Kuznetsov, A. A Synthetic Approach Towards Drug Modification: 2-Hydroxy-1-Naphthaldehyde Based Imine-Zwitterion Preparation, Single-Crystal Study, Hirshfeld Surface Analysis, and Computational Investigation. *RSC Adv.* **2024**, *14* (10), 6476–6493. https://doi.org/10.1039/D3RA08727A.
52. Tahir, M. N.; Rashid, Z.; Munawar, K. S.; Ashfaq, M.; Sultan, A.; Islam, M. S.; Lai, C. H. Synthesis, Characterization, and Exploration of Supramolecular Assembly in a 4-Aminophenazone Derivative: A Comprehensive Study Including Hirshfeld Surface Analysis, Computational Investigation, and Molecular Docking. *J. Mol. Struct.* **2024**, *1308*, 137953. https://doi.org/10.1016/j.molstruc.2024.137953.
53. McKinnon, J. J.; Jayatilaka, D.; Spackman, M. A. Towards Quantitative Analysis of Intermolecular Interactions with Hirshfeld Surfaces. *Chem. Comm.* **2007**, *53* (37), 3814–3816. https://doi.org/10.1039/B704980C.
54. Khan, O. *et al*. Synthesis, Single Crystal XRD, *In-Vitro*, and *In-Silico* Studies of Polysubstituted Tetrahydropyridine as α-Amylase Inhibitor. *J. Mol. Struct.* **2024**, *1305*, 137770. https://doi.org/10.1016/j.molstruc.2024.137770.
55. Jamil, S. *et al*. Benzimidazolium Quaternary Ammonium Salts: Synthesis, Single Crystal and Hirshfeld Surface Exploration Supported by Theoretical Analysis. *R. Soc. Open Sci.* **2024**, *11* (2), 231094. https://doi.org/10.1098/rsos.231094.
56. Jelsch, C.; Ejsmont, K.; Huder, L. The Enrichment Ratio of Atomic Contacts in Crystals, an Indicator Derived from the Hirshfeld Surface Analysis. *IUCrJ* **2014**, *1* (2), 119–128. https://doi.org/10.1107/S2052252514003327.
57. Turner, M. J.; McKinnon, J. J.; Jayatilaka, D.; Spackman, M. A. Visualisation and Characterisation of Voids in Crystalline Materials. *Cryst. Eng. Comm.* **2011**, *13* (6), 1804–1813. https://doi.org/10.1039/C0CE00683A.
58. Mackenzie, C. F.; Spackman, P. R.; Jayatilaka, D.; Spackman, M. A. CrystalExplorer Model Energies and Energy Frameworks: Extension to Metal Coordination Compounds, Organic Salts, Solvates and Open-Shell Systems. *IUCrJ* **2017**, *4* (5), 575–587. https://doi.org/10.1107/S205225251700848X.
59. Parveen, B.; Shahzadi, S.; Ali, S.; Feizi-Dehnayebi, M.; Munawar, K. S.; Ashfaq, M.; Tahir, M. N. Synthesis, Spectral Characterizations, Computational Studies and Biological Investigation of 4-(4-(2-Hydroxyethyl) Phenylamino)-4-Oxobutanoic Acid and its Trimethyltin(IV) Complex. *J. Mol. Struct.* **2024**, *1315*, 138851. https://doi.org/10.1016/j.molstruc.2024.138851.
60. Kurbanova, M.; Ashfaq, M.; Sadigova, A.; Feizi-Dehnayebi, M.; Maharramov, A.; Tahir, M. N. A Hydrazone Derivative: Synthesis, Crystal Structure, Supramolecular Assembly Exploration by Hirshfeld Surface Analysis and Computational Study. *J. Struct. Chem.* **2024**, *65* (1), 92–106. https://doi.org/10.1134/S0022476624010098.
61. Lanez, T.; Feizi-Dehnayebi, M.; Lanez, E. Assessment of the Electrostatic Binding of Ferrocenylmethyl-Nitroaniline Derivatives to DNA: A Combined Experimental and Theoretical Study. *J. Mol. Struct.* **2024**, *1308*, 138386. https://doi.org/10.1016/j.molstruc.2024.138386.
62. Sharmila, S.; Mahalakshmi, C. Homo Lumo Study, Reactivity Descriptors and Mulliken Charges of Imidazole Derivative. *IRJEdT* **2023**, *5* (4), 35–38.
63. Abu-Dief, A. M.; Omran, O. A.; Feizi-Dehnayebi, M.; Alqurashi, A.; Omar, I.; Alhashmialameer, D.; Mohamad, A. D. M. Fabrication, structural Elucidation, and DFT Calculation of Some New Hydrophilic Metal Chelates Based on N N′-(1-Methyl-2-Oxoindolin-3-Ylidene) Benzohydrazide Ligand: Pharmaceutical Studies and Molecular Docking Approach. *Appl. Organomet. Chem.* **2024**, *38* (9) e7593. https://doi.org/10.1002/aoc.7593.
64. Rossi, A.; Stagno, C.; Piperno, A.; Iraci, N.; Panseri, S.; Montesi, M.; Feizi-Dehnayebi, M.; Bassi, G.; Di Pietro, M. L.; Micale, N. Anticancer Activity and Morphological Analysis of Pt (II) Complexes: Their DFT Approach, Docking Simulation, and ADME-Tox Profiling. *Appl. Organomet. Chem.* **2024**, *38* (5), e7403. https://doi.org/10.1002/aoc.7403.
65. Majumdar, D.; Chatterjee, A.; Feizi-Dehnayebi, M.; Kiran, N. S.; Tüzün, B.; Mishra, D. 18-Aminoquinoline Derived Two Schiff Base Platforms: Synthesis, Characterization, DFT Insights, Corrosion Inhibitor, Molecular Docking, and pH-Dependent Antibacterial Study. *Heliyon* **2024**, *10* (15), e35591. https://doi.org/10.1016/j.heliyon.2024.e35591.